
Retinal oscillations carry visual information to cortex

Kilian Koepsell*, Xin Wang[†], Vishal Vaingankar[‡], Yichun Wei[‡], Qingbo Wang[‡],
Daniel L. Rathbun[‡], W. Martin Usrey[‡], Judith A. Hirsch[†] & Friedrich T. Sommer*

Abstract

Thalamic relay cells fire action potentials that transmit information from retina to cortex. The amount of information that spike trains encode is usually estimated from the precision of spike timing with respect to the stimulus. Sensory input, however, is only one factor that influences neural activity. For example, intrinsic dynamics, such as oscillations of networks of neurons, also modulate firing pattern. Here, we asked if retinal oscillations might help to convey information to neurons downstream. Specifically, we made whole-cell recordings from relay cells to reveal retinal inputs (EPSPs) and thalamic outputs (spikes) and analyzed these events with information theory. Our results show that thalamic spike trains operate as two multiplexed channels. One channel, which occupies a low frequency band (< 30 Hz), is encoded by average firing rate with respect to the stimulus and carries information about local changes in the image over time. The other operates in the gamma frequency band (40-80 Hz) and is encoded by spike time relative to the retinal oscillations. Because these oscillations involve extensive areas of the retina, it is likely that the second channel transmits information about global features of the visual scene. At times, the second channel conveyed even more information than the first.

Introduction

Thalamic relay cells transmit the information encoded in retinal firing rates downstream to cortex. It is widely held that the amount of information that retinal spikes carry is limited by the precision with which the firing rate tracks changes in the stimulus, a framework of stimulus-locked rate coding. Yet neural coding is not limited to stimulus-locked patterns of response; the dynamics of intrinsic networks (Brivanlou et al., 1998; Meister et al., 1995) also influences firing. Indeed, work in several modalities suggests that information can be encoded by spike timing with respect to ongoing oscillatory activity (Ahissar and Vaadia, 1990; Szwed et al., 2003; Friedrich et al., 2004; O'Keefe and Recce, 1993; Montemurro et al., 2008).

Oscillations in the firing rate of retinal ganglion cells are seen in species as diverse as the frog and cat (Arai et al., 2004; Heiss and Bornschein, 1965, 1966; Laufer and Verzeano, 1967; Castelo-Branco et al., 1998). A natural question is whether these intrinsic retinal rhythms might provide information to higher stages in the visual pathway. To address this subject, we made whole-cell recordings *in vivo* from the cat's lateral geniculate nucleus of the thalamus (LGN) during the presentation of natural movies. With this technique, it was possible to detect both individual retinal inputs and the spikes they evoke from single relay cells. In addition, we analyzed extracellular recordings of retinal

*Redwood Center for Theoretical Neuroscience, University of California Berkeley, 132 Barker Hall, MC #3190, Berkeley, CA 94720-3190, USA

[†]Neuroscience Graduate Program, University of Southern California, Los Angeles, CA, USA

[‡]Center for Neuroscience, University of California, Davis, CA, USA

activity obtained in a separate laboratory as a control. Thus far, our results show that oscillations in retinal inputs, EPSPs, can be transmitted to cortex by thalamic outputs, spikes.

We next used information theory to explore how both external visual stimuli and intrinsic rhythms modulate patterns of thalamic activity (for further details, see Koepsell and Sommer, 2008). Our analyses showed that these two components of the input a single thalamic neuron receives are multiplexed into two parallel channels. One channel is encoded by average firing rate with respect to the stimulus, stimulus-locked coding. It operates in the low frequency band (< 30 Hz) and carries information about sequential changes in the visual stimulus. The second channel is encoded by the timing of individual spikes relative to the retinal oscillations, oscillation-based coding. This channel operates in the gamma-frequency band (40-80 Hz) and, because oscillations involve distributed networks, is likely to convey information about large-scale features or spatiotemporal context. Remarkably, the amount of information in the second channel could match or even exceed that conveyed by the first. Further we were able to reproduce this result with a simple model of a relay cell. Thus, these two multiplexed channels are not, in principle, difficult to generate.

The presence of two information channels in the spike trains of single relay cell offers substantial advantages for transmission of information to the cortex. For example, dual channels could enhance robustness of the system to noise since they offer two mechanisms for decoding spike trains. Moreover, the second channel provides a conduit for novel information that is not conveyed by stimulus-locked changes in firing rate alone.

Results

The results were obtained from adult cats in two different laboratories, each using different recording techniques, visual stimuli and anesthetics. The main dataset includes whole-cell recordings from thalamic relay cells were made from 15 subjects. A second dataset, that served as a control, included extracellular recordings from retinal axons in the optic tract from 3 subjects.

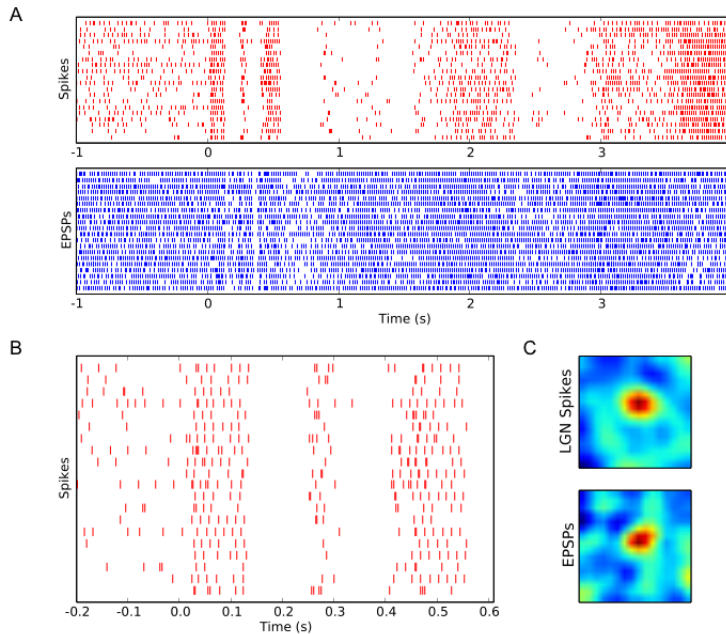


Figure 1: *Timing of retinogeniculate EPSPs and thalamic spikes recorded intracellularly from a single relay cell during the presentation of natural movies.* (A) Rasters of timings for spikes (red, top) and EPSPs (blue, bottom) in response to multiple trials of a movie clip that began at time $t=0$. (B) Raster for spike timings around the movie onset with higher resolution than in A. (C) Receptive fields for spikes (top) and EPSPs (bottom) mapped from responses to a movie; red indicates excitation to bright and blue excitation to dark.

The temporal structure of inputs and outputs of single relay cells

We focused our analyses on responses to natural movies, stimuli that reprise features present in the environment. In order to examine the relationship between the retinal inputs and thalamic outputs that these movies evoked, we used cluster analysis. This method allowed us to label excitatory synaptic potentials (EPSPs) in the intracellular signal and to separate these from spikes (Fig. 1A, top) are red and for EPSPs (Fig. 1A, bottom) are blue. Each row shows the response to a 5 s clip of the full stimulus. Raster plots show how inputs (EPSPs) and outputs (spikes) tracked changes in the stimulus; their rates systematically sped and slowed during repeated presentations of the same movie clip. An expanded view of the spike trains shows that there was a fair amount of jitter between one trial of the stimulus and the next; this variability is greater than that recorded for full field flicker (data not shown, and see Liu et al., 2001; Reinagel and Reid, 2000; Eckhorn and Popel, 1975). From the averaged rate over time we were able to extract the receptive fields from the response (Wang et al., 2007) for both the retinal inputs (Fig. 1C top) and the spikes (Fig. 1C, bottom). Both of the receptive fields have the round shape characteristic of ganglion cells. The shape of the receptive field of the inputs (Usrey et al., 1998) is consistent with the interpretation that they are retinogeniculate EPSPs fed forward from the retina rather than fed back from the cortex. This conclusion is supported by the prominent size of the events and the fast maintained firing rates (Frishman and Levine, 1983) (see Fig. 3A). Not only are unitary cortical inputs rarely big enough to visualize (Granseth and Lindstrom, 2003) unless the membrane resistance is made larger by blockade of potassium channels but cortical cells in layer 6 have very low maintained rates (Gilbert, 1977).

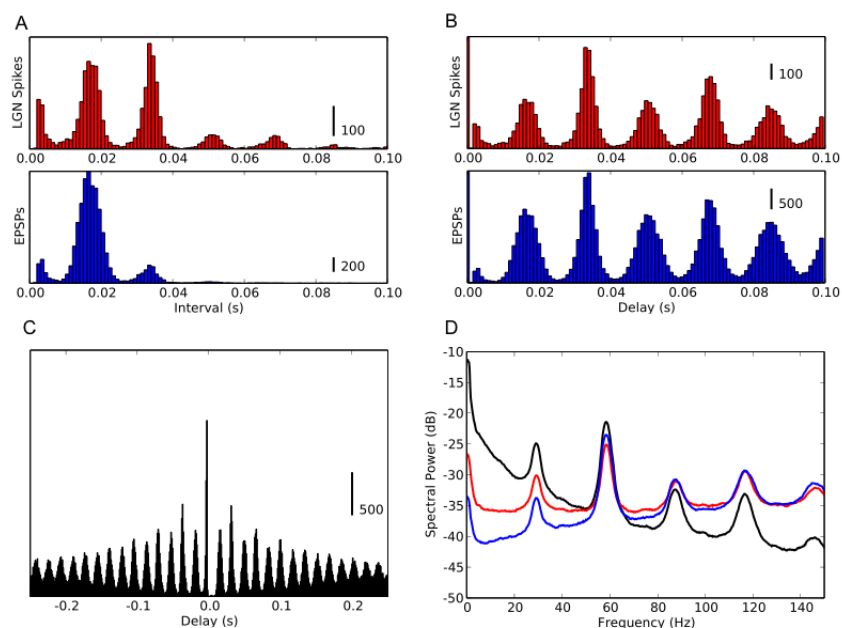


Figure 2: *Periodicity in timings of LGN spikes and EPSPs.* (A) Time-interval histogram for spikes (red, top) and EPSPs (blue, bottom). (B) Auto-correlation histogram for spikes (red, top) and EPSPs (blue, bottom). (C) Cross-correlation histogram between EPSPs and spikes (spike at $t = 0$). (D) Power spectra of membrane potential (black), spikes (red) and EPSPs (blue) of same cell as in A-C, computed with multitaper method.

Intrinsic rhythmic activity

Neural activity is dictated by a combination of external stimuli and internal dynamics. The event times shown in Fig. 1 were plotted with respect to the onset of the stimulus. We next plotted the data with respect to the interval between the spikes or EPSPs as inter-spike intervals (Fig. 2A) or auto-correlograms (2B). The multi-modal shapes of these time interval histograms revealed additional

temporal structure in the neural responses; the tall peak at 17 ms and lesser peaks at multiples of that value showed that both the EPSPs and spikes oscillated near 59 Hz, Fig. 2A. Further, cross correlation of the two sets of events revealed a sharp peak near zero (Fig. 2C), showing that thalamic spikes followed individual retinal EPSPs with millisecond delays. The oscillations are also visible in the power spectra for EPSPs (red), spikes (blue), and the membrane potential (black), Fig. 2D. These oscillations are not visible in the rasters shown in Fig. 1, because the intrinsic retinal rhythms are not synchronized with the stimulus.

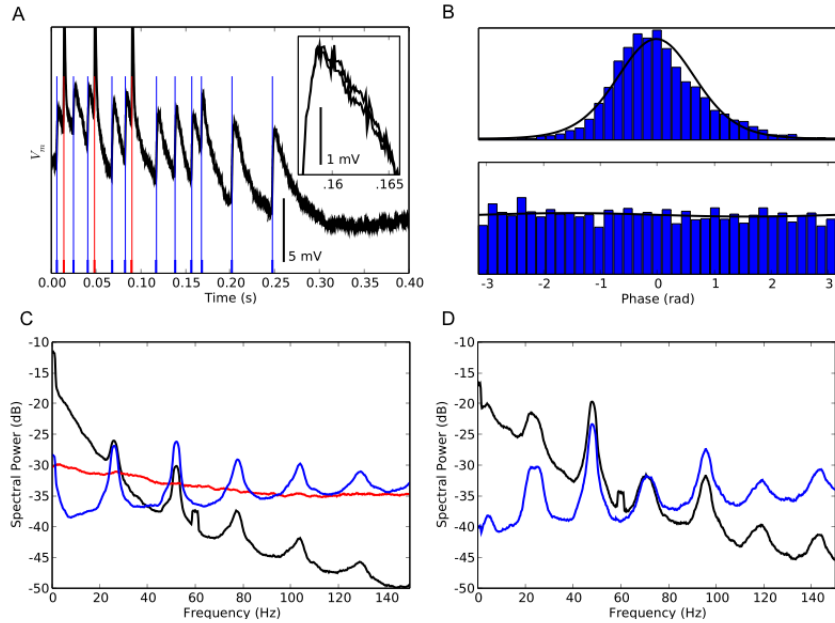


Figure 3: *Controls for stimulus and noise artifacts in recordings.* (A) Example of membrane voltage from a noisy recording before (gray trace) and after (black trace) removal of line noise (60 ± 0.1 Hz), see also magnified inset. The 60 Hz noise is visible, though far smaller than the biological signals. Vertical lines mark timings of detected spikes (red) and EPSPs (blue). (B) Phase distribution of EPSP events relative to band passed (51.5 ± 2 Hz) membrane potential (top) and relative to line noise (60 ± 0.1 Hz) component (bottom). (C) Spectra of membrane potential (black), spikes (red) and EPSPs (blue) during natural movie stimulation. (D) Spectra obtained from recordings of the same cell as in A with the eyes of the cat closed.

Since neural oscillations like that illustrated above often have frequencies in the gamma range, which includes power line frequencies (50 or 60 Hz) there is understandable concern that contamination of the biological signal can introduce false rhythms. Such concerns stem from experience with extracellular records in which spike heights often are on the order of tens of microvolts in amplitude, orders of magnitude smaller than the intracellular signals studied here.

Instances in which our recordings were contaminated with line noise provide useful controls for separating neural signal from electrical interference. An intracellular recording that included transients from the power line is overlaid with blue and red vertical lines that indicate the timings of EPSPs and spikes respectively, see Fig. 3A. The inset shows an overlay of an EPSP marred by the artifactual transient and of the same EPSP after notch filtering at 60 Hz. Except for the removal of the artifacts, the difference between the shapes of the EPSPs is negligible.

A separate analysis compared the relative timing of neural events to the oscillations we measured vs. their timing relative to the power line. If the neural events, EPSPs and spikes, locked selectively to the biological rhythms, then the distribution of event times plotted against phase of the intrinsic oscillations should have a strong peak. By contrast, a similar plot of event times with respect to the line frequency should be flat. These are exactly the distributions we observed, see Fig. 3B.

Another way to examine the consequences of contamination by the line power is to compare the power spectra of the raw signal to those of the event trains. The contribution of line noise is visible as a narrow peak at 60 Hz but is absent from the spectra of the EPSP and spike trains, see Fig. 3C.

There is also a possibility that the oscillations might simply reflect entrainment to the refresh rate of video display. We reduced this risk by using rapid video refresh rates, above 140 Hz (Wollman and Palmer, 1995; Williams et al., 2004; Butts et al., 2007). This tactic was successful, as shown by a comparison of recordings obtained during visual stimulation and those made when the eyes were occluded and the monitor switched off, see Fig. 3C and Fig. 3D. The spectra for the membrane potential (black) and EPSPs (blue) were similar; the cell fired too few spikes when the eye was closed to compute a spectrum.

Finally, to rule out the possibility that the oscillations were unique to our intracellular methods, we analyzed 20 extracellular recordings from retinothalamic axons in the optic tract obtained in a second laboratory. Gamma oscillations were present in recordings from this preparation, as depicted for one cell, see Fig. 4.

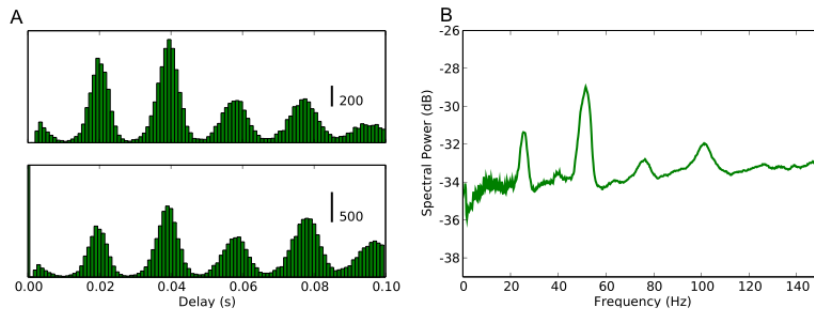


Figure 4: *Periodicity in spike timings of retinal ganglion cells.* (A) Time-interval histogram (top) and auto-correlation histogram (bottom) for spikes of a retinal ganglion cell from extracellular recording in optic tract. (B) Power spectrum of spike timings of the same cell as in A, computed with multitaper method.

Range of Oscillation Strengths

How can even small contributions of oscillatory activity be quantified? So far we have used simple measures that explore either the time domain (plots of inter-spike intervals and autocorrelations) or the frequency domain (power spectra). These measures provide a direct and intuitive means of displaying prominent oscillations. But the number and height of the peaks in plots of the inter-spike interval histograms or autocorrelograms lack the sensitivity to reveal weak oscillations. Further, power spectra often contain spurious peaks due to the refractoriness of the spiking process. Thus, we used the oscillation score (OS , see Methods and Muresan et al., 2008) to examine the strength and frequency of oscillations in the gamma range for three datasets: the whole cell recordings in current clamp we have discussed so far and two additional control groups. One control group comprised recordings made in voltage rather than current clamp mode (synaptic events are easier to detect in voltage clamp). The second control group was made of the extracellular recordings from the optic tract.

A scatter plot of oscillation score against frequency showed a range of oscillation strengths from weak to strong, see Fig. 5A. We included all cells in the analysis that oscillated with a consistent frequency ($\sigma_f < 4$ Hz across trials). Surrounding pairs of histograms of inter-spike interval (top) and autocorrelation functions (bottom) correspond to lettered points in the scatter plot and provide comparison of raw data from which those scores were derived, Figs. 5B-F). Note that there is a small but significant score for a cell whose inter-spike interval plot shows little evidence of oscillatory activity (Fig. 5F).

The values plotted in Fig. 5 are also summarized in Table 1. We usually recorded in voltage clamp mode, but singled out cells that seemed to oscillate for further analysis in current clamp. There is

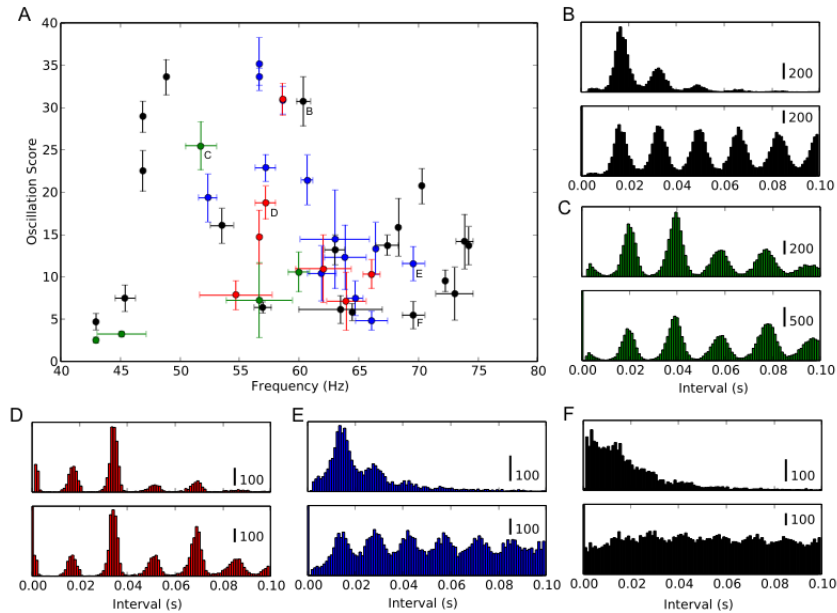


Figure 5: *Oscillations in population of all recorded cells.* (A) Oscillation strength quantified by oscillation score as a function of oscillation frequency for all recorded cells that show oscillatory behavior. LGN spike outputs are shown in red, LGN EPSPs in blue, EPSCs from LGN voltage clamp recordings in black, and retinal ganglion spikes from optic tract recordings in green. The labeled points refer to the examples in panel B-F. (B)-(F) Examples of spike interval histograms (top) and auto-correlation histograms (bottom) for cells with different oscillation score. Color convention as in A.

modest discrepancy between the frequency of oscillations from the extracellular retinal and intracellular thalamic records. This difference might reflect differences in sampling bias, visual stimuli (natural movies for the intracellular experiments and m-sequences for the extracellular experiments), or anesthetic (thiopental, a barbiturate, for the extracellular experiments and, propofol, a new class of anesthetic, for the intracellular experiments; note, however, that oscillations have been observed in awake cats (Doty et al., 1964; Heiss and Bornschein, 1965, 1966)). It is also possible that differences reflect a circuit property of the thalamus; relay cells often receive input from several ganglion cells (Hamos et al., 1985; Usrey et al., 1999). If only one of several inputs to a relay cell oscillated, we would have scored that relay cell as oscillatory even if its other retinal inputs fired aperiodically. There also was a larger percentage of oscillating EPSP than spike trains; this difference reflects the limitation of the oscillation score measure for very low spike rates.

Analyses of information content

Having established the presence of an oscillatory component of retinogeniculate responses, we began our analyses of the information content in retinal and thalamic event trains. The first analyses were made from the perspective of stimulus-locked coding, using the current clamp recordings. We estimated lower and upper bounds for the amount of information that could be transmitted by changes in event rate that recurred across repeated presentations of the same stimulus. In order to obtain each bound, it was necessary to use separate methods (Bialek et al., 1991). To establish the upper bound, we decomposed the power spectrum of the spike trains into two components. One component represented the part of the response that was consistent across stimulus trials, typically equated with the signal (Fig. 6A, top, solid curve) and the other corresponded to the variation in response across trials, usually taken as noise, (Fig. 6A, top, dotted curve). The information rate, calculated from the area under the solid curve in Fig. 6A bottom, was 0.4 bit/spike. We established the lower bound by determining how well the visual stimulus could be reconstructed from the convolu-

Table 1: Oscillations in different datasets

		# cells in data set	# cells with consistent osc. ($\sigma_f < 4$ Hz)	# cells with strong osc. ($OS > 15$)
Current clamp recordings	Retinothalamic EPSPs	20	13 (65%)	7 (35%)
	Thalamic spikes	20	6 (30%)	2 (10%)
Control recordings	Retinothalamic EPSCs recorded only in voltage clamp	30	19 (63%)	7 (23%)
	Retinal spikes from the optic tract	20	5 (25%)	1 (5%)

tion of the cellular response with the receptive field (Fig. 6B, and Methods). For this case, the signal is the reconstruction of the receptive field and the noise is the deviation of the reconstruction and the stimulus. The information rate calculated from this second method was 0.3 bit/spike, Fig. 6B, bottom. The values for upper and lower bounds are similar to those reported previously (Liu et al., 2001; Reinagel and Reid, 2000; Eckhorn and Popel, 1975).

The information rates estimated above were made with the widely used entropy methods for a Gaussian information channel, which assumes that signal and noise are Gaussian (Borst and Theunissen, 1999). We also estimated information rates using the direct method for single spike information (Brenner et al., 2000), which is valid for arbitrary distributions but assumes that single spikes encode information independently (Figs. 6C, D). The direct method, however, requires so much data to make estimates at fine times scales that it is common to obtain estimates by extrapolating from values obtained at coarser time scales (wider bins, Fig. 6C). The estimates obtained using the entropy method, 0.4 bit/s and the direct method, 0.58 bit/s were very close. The similarity of these two values, each obtained with a different, complementary, method, suggests that they reflect the true information rate.

The results plotted in Fig. 6 illustrate an important aspect of how relay cells use stimulus-locked rate coding to encode visual signals. The information about temporal changes in the stimulus peaked at low frequency and dropped sharply at a cut-off frequency below 30 Hz (Fig. 6A and 6B). The shape of this distribution reflects not only the intrinsic properties of thalamic circuits but also the statistics of natural images, which are skewed to low spatial and temporal frequencies (Ruderman and Bialek, 1994). This finding is consistent with previous studies that used natural scenes (Dan et al., 1996) rather than flickering, full-field stimuli (Reinagel and Reid, 2000; Liu et al., 2001).

The prominence of the oscillations in the "noise" motivated us to ask if it might actually encode information hidden from conventional analyses. Answering this question required that we measure the degree to which the oscillations contributed to the variance of the stimulus-locked response. We estimated the instantaneous phase of the retinal oscillations (EPSPs) as the complex angle of an analytical signal calculated by convolving a Morlet wavelet (Fig. 7A top, inset) with the event train (blue ticks in Fig. 7A); and see Methods. The resulting waveform (blue ripple, Fig. 7A bottom) was then used to determine the phases at which the relay cell spiked (red ticks, Fig. 7A, bottom). This analysis showed that the phase locking between retina and thalamus was strong, as made clear by the tall peak in the phase histogram plotted in Fig. 7B top. There was no evidence, however, that each new trial of the stimulus set the absolute phase of the neural response: when we used the estimated phase for inputs in one trial to determine the phase of spikes in the next, the resulting distribution (the shift predictor) was flat (Fig. 7B, bottom).

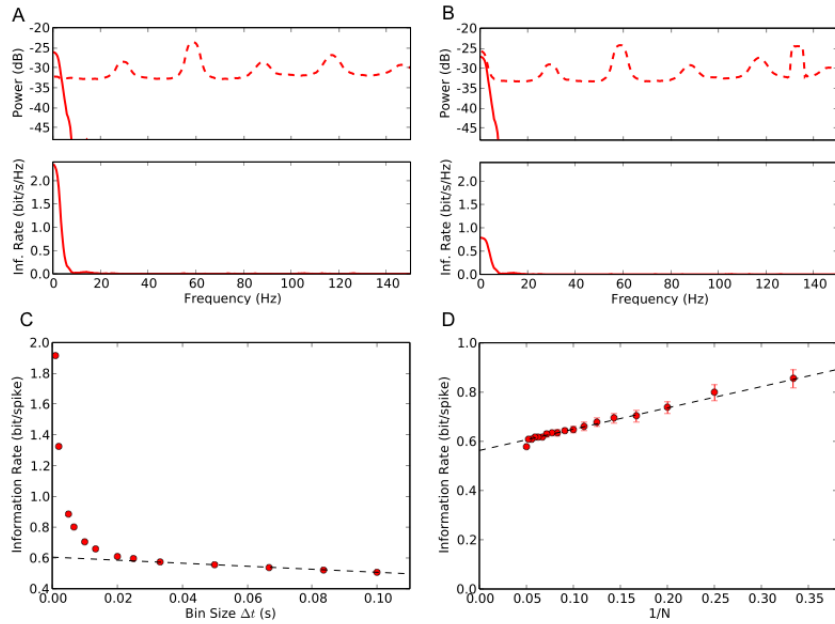


Figure 6: *Estimates for information rate of LGN spikes.* (A) Power spectrum (top) of LGN spike response decomposed into signal (red line) and noise (dashed line) and spectral information rate (bottom) as upper bound for the transmitted information; the total information rate given by the area under the curves is 8.3 bit/s. With a mean spike rate of 19 spikes/s, this corresponds to 0.4 bit/spike. (B) Power spectrum (top) of LGN spike response decomposed into signal (red line) and noise (dashed line) with the stimulus reconstruction method as lower bound for the transmitted information; the estimated information rate is 5.7 bit/s or 0.3 bit/spike, similar to values measured previously (Liu et al., 2001; Reinagel and Reid, 2000; Eckhorn and Popel, 1975). (C) Information per spike as a function of bin width Δt . Linear extrapolation ($\Delta t \rightarrow 0$) yields an information rate of 0.58 bit/spike. (D) Direct information estimate as a function of number of trials N . Linear extrapolation ($\Delta t, 1/N \rightarrow 0$) yields 0.56 bit/spike.

We further quantified the degree to which the thalamic spikes locked to the retinal inputs with a concentration parameter κ of a von Mises distribution that we fitted to each phase histogram (see Fig. 7B, Methods). The concentration parameter is zero for a flat phase distribution and increases with increasing degree of phase locking between retinal input and thalamic output. Thus fits with the tallest peaks indicate the highest degree of phase locking and the most reliable transmission of oscillations in the inputs (Fig. 7B, inset). The value for this cell was 2.3 and the range for all cells was 0 – 3.1.

Next we used our method of estimating the phases of the retinal oscillations to align the phases of EPSPs over different trials. This allowed us to explore how the random phases of oscillations across trials might have introduced jitter and hence decreased precision in the stimulus-locked response. To align the phase of the responses across trials, we measured the local phase of ongoing activity recorded just before each repeat and adjusted that phase to match the mean phase (see Methods). The alignment to the instantaneous phase reduced the jitter in the cross-trial latencies to a striking extent. Remarkably, what had seemed to be randomly distributed events in the actual recordings (Fig. 7C) assumed temporally precise patterns in the de-jittered traces (Fig. 7D). Much of the variation across trials that had seemed like random jitter had come from periodic activity. To address directly the question of whether the oscillatory activity in the gamma band could be used to transmit visual information, we aligned the phases of the EPSPs within the complete dataset. Rather than realigning phases at the start of each trial, as above, we made an alignment each time the local phase of the response deviated markedly from the reference (see Methods); the power spectrum of the de-jittered records, decomposed into signal and noise, is plotted in Fig. 7E, top. Afterwards, we analyzed the

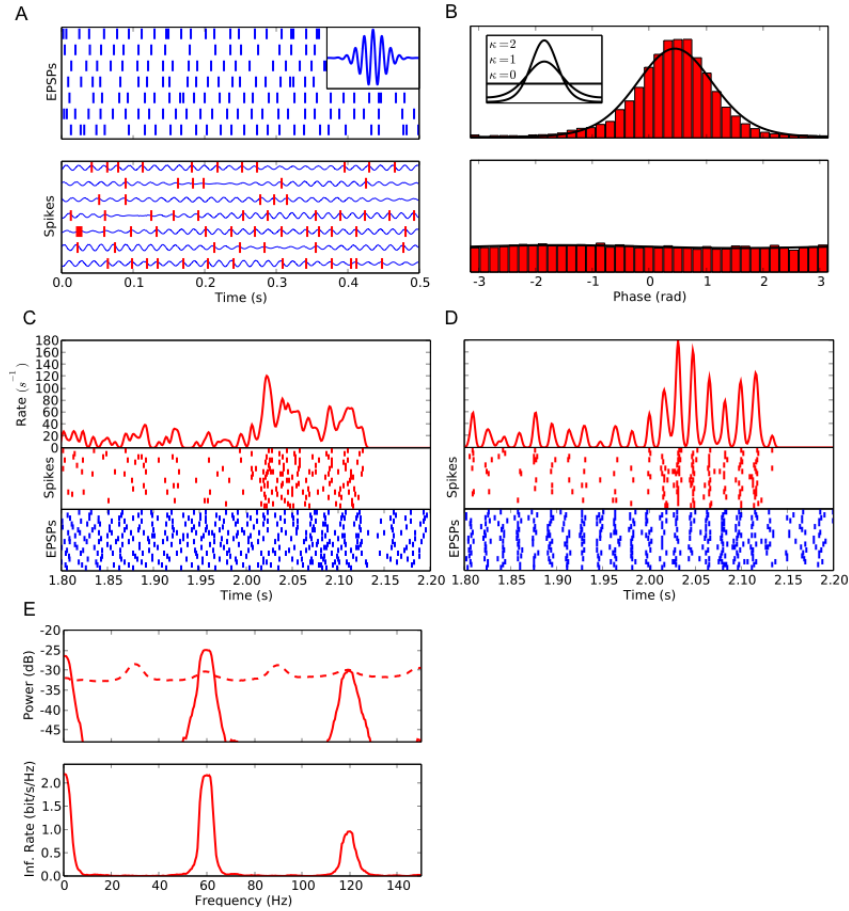


Figure 7: *Adjusting response latency based on the phase of ongoing oscillations reduces temporal jitter in spike timings across trials.* (A) EPSP trains (top) and spikes (bottom, red) for 7 trials, analytical signal (bottom, blue curve) computed from EPSP trains of each trial by filtering with a Morlet wavelet (inset). (B) Histogram of spike phases (top) and shift predictor (bottom) for an oscillation frequency of 59 Hz. (C) Response recorded with fixed latency to stimulus onset. Averaged spike rate (red curve) and rasters for spikes (red) and EPSPs (blue) for 20 trials of a movie clip. Spikes rasters were smoothed with Gaussian window ($\sigma = 2$ ms) before averaging. (D) Responses corrected for latency variations up to ± 10 ms by using periodicity in the ongoing activity that preceded stimulus onset; conventions as in A. (E) Power spectrum (top) of de-jittered spike train decomposed into signal (solid line) and noise (dashed line) for single cell and spectral information rate (bottom). De-jittering increased the total information from 0.3 - 0.4 bit/spike (Fig. 6A/B) to 1.6 bit/spike.

de-jittered dataset by using information theory just as we had done for the raw recordings. The de-jittering exposed additional bands near 60 Hz and 120 Hz that had high signal to noise ratios, Fig. 7E bottom, but left the low frequency, 30Hz, band used for stimulus- locked coding intact. When the additional bands were taken into account, the upper bound on the rate of information available from the spike train quadrupled; it grew from 0.4 to 1.6 bit/spike. This gain in information is possible because the band carrying stimulus locked information is separate from the bands that carry the oscillation based information. If spectra of the extrinsic and intrinsically patterns of activity had overlapped, then oscillations would have interfered with the information transmitted by the thalamic spike train.

Across the population, the amount of information available in the second channel depended on the strength of the retinal oscillations. There was pronounced phase-locking of retinal inputs to a wide range of gamma oscillations, as shown in a plot of concentration parameter against fre-

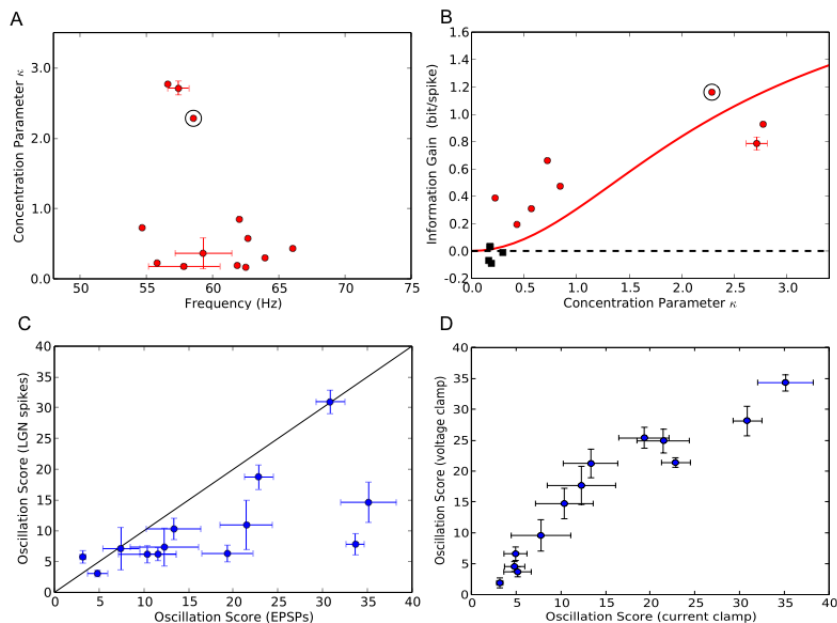


Figure 8: *Population results for phase locking, information gain and oscillation score.* (A) Phase-locking of thalamic spikes for all (13/20) cells that had oscillating EPSP trains (see Table 1). Error bars indicate standard deviation when multiple movies were presented; circled point denotes the cell analyzed in Figs. 1,2,6,7. (B) Gain in information rate after de-jittering plotted against concentration parameter κ ; conventions as in A. For 8 of 20 cells (red points), the information increased significantly ($p < 0.05$, computed using permutation test) after de-jittering of the spike train (see A). Red curve depicts gain in transmitted information predicted by our model (Fig. 9) for variable κ . (C) Oscillation score of LGN outputs (spikes) as a function of oscillation score of LGN inputs (EPSPs). (D) Oscillation scores of inputs to LGN cells (EPSCs, EPSPs): score of the voltage clamp recording shown as function of the score of the current clamp recording.

quency (Fig. 8A). The gain in information after de-jittering was large for cells with strong oscillations and commensurately smaller for cells with weaker oscillations, red points in Fig. 8B. Here, as for Figs. 6A and 7E, we estimated the information using the entropy method for the Gaussian information channel. We chose this method because temporal realignments of the spikes were so small, < 20 ms, that the amount of data required for the more general direct method (see Methods) was unfeasibly large (see Fig. 6C). The red curve is a prediction of information gain as a function of the concentration parameter; it was generated with a computational model we describe below and calculated with the direct method. Panel 8C explores the relationship between oscillation scores for EPSPs vs. the spikes they evoke. Most points fall on or below the line of unity slope; as mentioned earlier, the relatively reduced scores for the spikes reflect limitations in the oscillation score measure for low spikes rates in our recordings. Last, we obtained voltage-clamp recordings from many cells; the oscillation scores calculated for the EPSCs in these data are similar to those obtained from recordings made in current clamp (Fig. 8D).

Modeling the multiplexed channels

Thus far, our analyses suggest that many thalamic relay cells convey information about natural stimuli via spike trains that are multiplexed between two channels that operate on different time scales. One channel encodes information by modulations in spike rate determined by changes in the stimulus and uses the frequency band below 30 Hz. A second channel utilizes spike timing to convey information about ongoing retinal activity. This channel uses higher, gamma band, frequencies. In order to understand how this dual mode of transmission might be formed, we built a simple model (Fig. 9A, see Methods and Koepsell and Sommer, 2008). Thalamic spikes were generated by

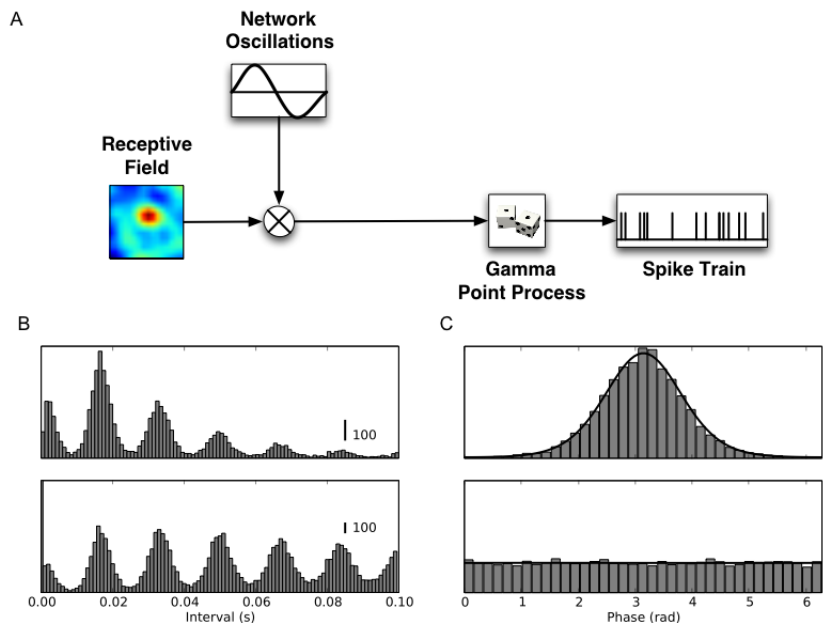


Figure 9: *Quasi-periodic gamma (QPG) model reproduces spike timing statistics and phase distribution.* (A) QPG model of the thalamic neuron that predicts spike statistics and information rate: Spike times are described by inhomogeneous gamma process. Spike rate is the product of two signals, the visual response evoked through the receptive field and a periodic signal that simulates ongoing retinal activity. (B) Simulated spike interval distribution (top) and auto-correlation histogram (bottom). (C) Simulated spike phase distribution (top) and shift predictor (bottom).

an inhomogeneous gamma process whose rate was determined by a combination of two signals, one that corresponded to visual input filtered by the receptive field and another that represented retinal oscillations. The signals were combined by multiplication to reproduce the amplitude modulation seen in event rates of the de-jittered recording (i.e. Fig. 7D). Although our model had only four free parameters, the order of the gamma process, the concentration parameter, the oscillation frequency and the bandwidth, it was able to reproduce the key aspects of the results. These features include inter-spike intervals and phase-locking (compare Fig. 9B with 2B) and the power spectra and information content of the raw (compare Fig. 6 and 10A, and C) de-jittered spike trains (compare Figs. 7E with 10B). The simplicity of our model suggests that complicated mechanisms are not required to generate the multiplexed channels.

Discussion

We provide experimental evidence that individual retinal ganglion cells multiplex two streams of information via the thalamus to cortex. One stream is well known and encodes visual information by changes in firing rate that are time-locked to external visual stimuli. The second, novel, channel encodes information by aligning spike timing to intrinsic retinal oscillations. We were able to expose this additional channel by developing a technique for measuring the phase alignment of spikes fired by single relay cells to the local phase of oscillations in presynaptic retinal input (see Koepsell and Sommer, 2008). Because this oscillation-based channel operates in a frequency band separate from that containing the stimulus-locked channel, it adds to the total amount of information transmitted to cortex. The amount of extra information the second channel provides increases as a function of oscillation strength and can as much as triple the number of bits that each spike carries. Further these results are easily reproduced by a simple computational model.

What information might the second channel encode? It is likely, that the oscillation based channel transmits contextual information about the stimulus. Oscillatory activity in retina is generated by the

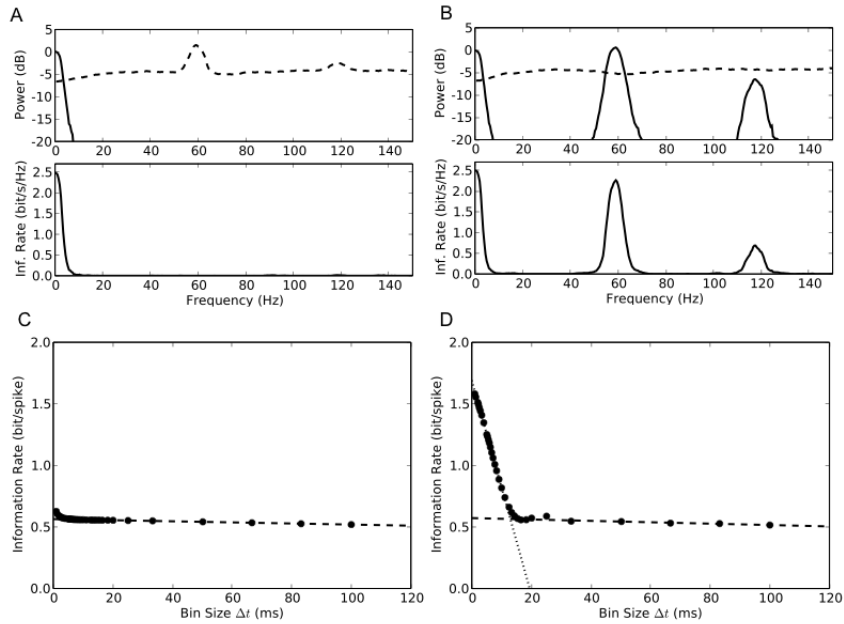


Figure 10: *Information rate for QPG model.* (A) Simulation with random oscillation phase across different trials: Signal spectrum (top, solid line), noise spectrum (top, dashed line) and information estimate (bottom). (B) Simulation with oscillation phase aligned across different trials: Signal spectrum (top, solid line), noise spectrum (top, dashed line) and information estimate (bottom). (C) Information estimate with oscillation phase randomized across trials (0.6 bit/spike). (D) Information estimate with oscillation phase aligned across trials increases from 0.6 bit/spike to 1.8 bit/spike if small bin width (< 20 ms) are taken into account.

coordinated activity of distributed networks that span large regions of retinal, hence visual, space. Previous studies have shown that extended visual contours can synchronize oscillations among distant ganglion cells (Neuenschwander and Singer, 1996; Stephens et al., 2006). Thus, global features might modulate the frequency or amplitude of retinal oscillations or the alignment of thalamic spikes to the phase of the retinal oscillations. Hence, the oscillation-based channel might serve to convey large-scale information such as the overall gist of a scene (Navon, 1977; Torralba, 2003). The information that this channel transmits might be unique or might complement information about spatial structure that is available in the relative timing of action potentials fired by a single neuron (McClurkin et al., 1991; Klein, 1992; Reich et al., 1997) or differences in the relative timing of parallel spike trains with respect to visually evoked response latency (Gollisch and Meister, 2008). The prediction that oscillations convey such contextual information is supported by recent experiments in frog. Blockade of retinal oscillations abolishes escape behavior elicited by large stimuli that mimic predators but does not impair detection of punctuate objects that resemble prey (Ishikane et al., 2005). Thus the use of oscillations to encode large-scale aspects of the visual scene might be evolutionarily conserved in the visual system.

If, however, the oscillations were not modulated by the visual stimulus, as in our model, they would still benefit visual processing. For example, synchronization due to oscillations can reduce the probability of errors made in encoding local features (Kenyon et al., 2004). As well, they might help transmit information effectively to the cortex, as follows. Retinal ganglion cells often diverge to synapse with multiple relay cells (Hamos et al., 1985; Usrey et al., 1999). In turn, relay cells that receive common retinal input often synapse with the same cortical target. The impact of each spike a relay cell fires depends on physiological context: coincident inputs are more likely to trigger a cortical spike than those that arrive at intervals longer than a few ms (Usrey et al., 1998; Bruno and Sakmann, 2006). Thus, oscillations might synchronize the arrival of converging thalamic inputs onto a common cortical target.

The presence of two channels that carry information could provide further advantage by conveying redundant information about the visual stimulus in separate frequency bands, as follows. The first copy is encoded by a straightforward mechanism, stimulus-locked changes in spike rate. To explain how the second copy is conveyed, we use the analogy of AM radio transmission. Here the visual signal modulates the amplitude of the higher frequency carrier, which, in this case, is the gamma oscillation. Thus, the visual stimulus is encoded redundantly, in two separate frequency bands of the thalamic spike train.

This redundancy increases robustness to noise since it provides two alternatives for cortex to decode the spike train, low passing or band passing. The low passed information would be read by conventional mechanisms of synaptic integration. The band-pass receiver is formed by cortical oscillations in the gamma band (Nowak et al., 1997; Hutcheon and Yarom, 2000; Fellous et al., 2001). Thalamic volleys that arrive nearer the peaks of the cortical oscillations, when cortical neurons are most depolarized, would be most likely to evoke spikes. This same scenario has been suggested to explain how oscillations propagate active from one cortical area to the next. Since the strength and frequency of gamma oscillations in cortex is increased by attention, the contributions of the novel channel might be enhanced during times of heightened vigilance to visual signals (Fries et al., 2007).

Methods

Preparation, stimulation and recording for whole-cell experiments

Adult cats (1.5 - 3.5 kg) were prepared as described earlier (Hirsch et al., 1998) except anesthesia was maintained with propofol and sufentanil. Whole-cell recordings of the membrane voltage or current were made with dye filled pipettes from 17 cells in 9 animals using standard techniques (Hirsch et al., 1998) (Axopatch 200A amplifier, Axon Instruments, Inc., Union City, CA) and digitized at 10 kHz (power1401 data acquisition system, Cambridge Electronic Design Ltd., Cambridge, UK). The stimuli were various natural movies (30 s duration) that were repeated 5-50 times. The movies were displayed at 19-50 frames per second on a video monitor (refresh rate 133-160 Hz) by means of a stimulus generator (VSG2/5 or ViSaGe, Cambridge Research Systems Ltd., Rochester, UK). Housing, surgical and recording procedures were in accordance with the National Institutes of Health guidelines and the University of Southern California Institutional Animal Care and Use Committee.

Preparation, stimulation and recording for extracellular experiments

Adult cats were prepared and anesthetized as described earlier (Usrey et al., 1998). The stimuli were white noise (m-sequences, see Usrey et al., 1998) created with a VSG2/5 visual stimulus generator (Cambridge Research Systems Ltd., Rochester, UK) and updated at the 140 Hz refresh rate of the video display. Spike trains were digitized at 20 kHz (power1401 data acquisition system, Cambridge Electronic Design Ltd., Cambridge, UK) and stored for further analysis. All procedures conformed to NIH guidelines and were approved by the institutional Animal Care and Use Committee at the University of California, Davis.

Event detection and sorting

Potential events (spikes, EPSPs and false positives) were detected as zero-crossings (from positive to negative) in the second derivative of the intracellular signal. Spikes were distinguished from EPSPs by a threshold criterion. A clustering algorithm (Harris et al., 2000) was used to separate EPSPs from false positives; each event was characterized using a short segment (1.5ms) of the second derivative. The first three principal components (in the space of the event-centered second derivative) were used as features in the clustering procedure; then clusters that corresponded clearly to retinal EPSPs as determined by visual inspection were selected for further analysis (Wang et al., 2007). The extracted spike trains of the LGN cell (red) and the event trains of the synaptic inputs (EPSPs) corresponding to retinal spikes (blue) are displayed in Fig. 1A,B.

Estimating receptive fields

We estimated the spatio-temporal receptive fields of the relay cells by using a model that predicted neural responses to the natural movies (Fig. 1C). Specifically we used regularized gradient descent (Machens et al., 2004) to optimize a linear convolution kernel with respect to the quadratic error between predicted and empirical response. The firing rates used to calculate the receptive fields were estimated with a temporal Gaussian filter, 25 ms half-width and spontaneous rates were taken as the average rate across the entire recording (Wang et al., 2007).

Estimating power spectra and information rate

Upper and lower bounds on the information rate in Fig. 6, Figs. 7E and Fig. 10 were estimated by the dynamic Gaussian channel based on the power spectrum and double checked with the direct method. We used a multitaper method (Jarvis and Mitra, 2001), with 5 tapers, on non-overlapping windows to estimate spectral power (Fig. 2D). These methods were based on different assumptions about the statistics of the stimulus and the response as well as the neural model (for overview, see Borst and Theunissen, 1999).

Estimating information rate: the Gaussian channel

When the signal has Gaussian statistics and the noise is additive and Gaussian, information rates can be calculated as (Bialek et al., 1991; Rieke et al., 1999):

$$I_G = \frac{1}{2} \int_{-\infty}^{\infty} \frac{d\omega}{2\pi} \log [1 + SNR(\omega)] \text{ bit/s}, \quad (1)$$

where $SNR(\omega) = S(\omega)/N(\omega)$ is the signal-to-noise ratio, computed in the frequency domain from the spectrum of the signal $S(\omega)$ and the spectrum of the noise $N(\omega)$. When different definitions of signal and noise were used, this formula yielded estimates for the upper and lower bounds for the information rate, as below:

Upper bound

The signal was defined as the component of the neural response that contained information about the stimulus (determined by cross-trial average of spike trains). The noise was defined as the deviation of individual trials from the average. Power spectra were estimated using the multi-taper method. Errors due to finite sample size (N) were corrected by assuming that the power of Gaussian noise decreases as $1/N$ in the average across trials (Sahani and Linden, 2003). With these definitions, the formula for the Gaussian channel gave estimates of an upper bound for the information that could be transmitted by stimulus-locked coding (see also Fig. 6A, Fig. 7E, Figs. 10A,B).

Lower bound (Reconstruction method)

The signal was defined as the stimulus (the movie) and the noise as the deviation between the actual stimulus and one that was reconstructed as follows. To reconstruct the stimulus, the neural spike train was convolved with a receptive field estimated from responses to a different movie (see above). With these definitions, the formula for the Gaussian channel gave a lower bound for the information that stimulus-locked coding could transmit (see Fig. 6B). Note that the estimate of the lower bound is tight only if the linear model used to reconstruct the stimulus captures the response of the neuron well.

Using the direct method to estimate information rates

So far, we have made that assumption that both the signal and noise are Gaussian. If, however, the noise is not additive nor Gaussian, then I_G does not guarantee an upper bound. Similarly, if the signal is not Gaussian, then I_G does not guarantee a lower bound. Therefore, to assess how well the Gaussian channel was able to capture the rates of information that relay cells actually transmitted, we used a technique called the “*direct method*”. This method does not rely on Gaussian statistics or any given neural model to estimate the total entropy in a neuron’s response. If it is assumed that all information is conveyed by single spikes rather than firing patterns, then the information that each

spike transmits is given by the formula (Brenner et al., 2000)

$$I = \frac{1}{T} \int_0^T dt \frac{r(t)}{\bar{r}} \log_2 \left[\frac{r(t)}{\bar{r}} \right] \text{ bit/spike}, \quad (2)$$

where $r(t)$ is the spike rate and \bar{r} is the mean rate averaged over the whole recording time T .

The direct method has a weakness, however; the accuracy of the estimate it provides depends on the bin width, Δt , used to compute the integral in the equation directly above. Specifically, the estimate converges to the true entropy only asymptotically (limit of zero bin width and infinite number of trials). Thus, narrow bins and finite data result in a pronounced overestimation of the amount of information that a cell transmits, see Fig. 6C, red dots.

The estimate can be improved by a linear extrapolation ($\Delta t \rightarrow 0$) of the values for larger bin sizes, Fig. 6C, dashed line. A similar extrapolation must be made for estimating information with an infinite number of trials, see Fig. 6D. The resulting value of 0.58 bit/spike was similar to the estimates obtained using the Gaussian channel (upper bound: 0.44 bit/spike, lower bound 0.30 bit/spike). Two factors probably account for the overestimation produced by the direct method. First, the number of trials (20) was limited; increasing the number of trials (N) by linear extrapolation ($\Delta t, 1/N \rightarrow 0$) yielded 0.55 bit/spike (Fig. 6D, dashed line). Second, the direct estimate did not remove redundancies due to correlations between single spikes.

Oscillation score

Muresan et. al (Muresan et al., 2008) used both the time and frequency domain to devise a new metric for the strength and frequency of oscillations. Their method to compute an ‘oscillation score’ (OS) applies a Fourier transform on an autocorrelation that is smoothed and whose central peak, including adjacent troughs due to the refractory period, is subtracted; these precautions remove confounds from the refractory period.

Quantification of the phase locking of spikes

To characterize periodicity in trains of unitary events (EPSPs, spikes) it was necessary to estimate frequency and phase at each point in time. Hence, we computed the complex analytic signal $A(t) = A_0(t) \exp(i\phi(t))$ by convolving the EPSP event train with a complex Morlet wavelet

$$w(t, f) = C \exp(2\pi i f t) \exp(-t^2/2\sigma_t^2)$$

centered at a frequency f with temporal width σ_t and normalization factor C (Fig. 7A). The amplitude A_0 of the analytic signal corresponded to the local power in the frequency band centered at f with bandwidth $\sigma_f = 1/(2\pi\sigma_t)$. The bandwidth we chose, $\sigma_f = 2$ Hz, corresponded to the width of the peak in the power spectrum and a temporal width of $\sigma_t = 80$ ms. The instantaneous phase $\phi(t)$ was estimated as the complex angle of the analytic signal and was used to measure the distribution of phases for membrane events (Fig. 3B, Fig. 7B, Fig. 9C). The phase distribution of spikes (Fig. 7B) was fitted with a von Mises (or cyclic Gaussian) distribution

$$M(\phi|\kappa, \mu) = e^{\kappa \cos(\phi - \mu)} / (2\pi I_0(\kappa)).$$

The mean phase μ was computed from the first trigonometric moment of the spike distribution

$$\langle \exp(i\phi) \rangle = \frac{1}{N} \sum_{n=1}^N \exp(i\phi(t_n)) = r \exp(i\mu).$$

The concentration parameter κ characterizing the width of the von Mises distribution was obtained by numerical solution of the equation $I_1(\kappa)/I_0(\kappa) = r$, where I_0 and I_1 were the modified Bessel functions of zeroth and first order. The concentration parameter κ is a measure of phase locking; the phase distribution becomes uniform for $\kappa \rightarrow 0$ and approaches a Gaussian distribution with variance $\sigma^2 = 1/\kappa$ for large κ .

Information in oscillatory spike trains

The estimated phase $\phi(t)$ of retinal oscillation at the time of stimulus onset, t , was used to align the timing of thalamic spikes across all trials by shifting each trial in time, $-\phi(t)/(2\pi f)$ (the absolute

value was < 10 ms). Thus, the phase of the retinal oscillations, which had been randomly distributed across trials, was made the same for each one 3). This alignment was made once for each cycle of the retinal oscillation in order to “de-jitter” the entire thalamic spike train (see Fig. 3D). Note that our method of de-jittering differs from those that use the stimulus (Aldworth et al., 2005) or the spike train itself (Richmond et al., 1990) as references in time. After aligning phases, we used equation (1) to provide an estimate of information rate that included the contribution of oscillations that were not locked to the stimulus. This method has been verified previously (Koepsell and Sommer, 2008) by expanding the direct method of estimating information rates for single spikes to take the phase of oscillations into account.

Simulation Experiments

Recently, (Koepsell and Sommer, 2008) we designed the *quasi-periodic gamma (QPG) model* to understand how the two different information channels might be multiplexed in the response of relay cells, (Fig. 9A): The QPG model describes spike generation by an inhomogeneous Gamma process (Barlow et al., 1957) with a factorial instantaneous rate. The conditional probability of generating a new spike at time t_i , given the last spike at time t_{i-1} is written as (Barbieri et al., 2001)

$$p_t(t_i|t_{i-1}) = \frac{k\lambda(t_i)}{\Gamma(k)} \left[k \int_{t_{i-1}}^{t_i} \lambda(u) du \right]^{k-1} \exp \left\{ -k \int_{t_{i-1}}^{t_i} \lambda(u) du \right\},$$

where k is the shape parameter of the gamma distribution, $\Gamma(k)$ is the gamma function, and the instantaneous rate $\lambda(t)$ is given by the product

$$\lambda(t) = 2\pi(RF \otimes s(t))M(\phi(t); \kappa, \mu).$$

The first factor $RF \otimes s(t)$ is the averaged firing rate calculated by convolving the stimulus with the receptive field, estimated as above). The second factor is a von Mises distribution $M(\phi; \kappa, \mu)$ that describes the periodic activity in single trials. The instantaneous phase of the periodic activity, $\phi(t)$, is given by the phase a random band-pass signal with frequency $f \pm \sigma_f$. All told, in addition to the parameters describing the receptive field, the model has four free parameters: k , κ , f , σ_f . (An additional degree of freedom, the mean phase, was arbitrarily set to $\mu=0$).

Fitting the model parameters

To assess how well the results in Figs. 1-8 were captured by the QPG model, we fitted the free parameters of the model to match the properties of the cell whose responses are indicated by the circled points in Figs. 8A, B. The concentration parameter κ was determined by fitting the von Mises distribution (Fig. 7B) to the phase distribution of the cell’s spikes and the parameters f and σ_f were fitted to the spectrogram of the spikes (see section). The shape parameter k of the Gamma process was determined as follows. The averaged rate $\lambda_0(t)$ was estimated from the average of the neural responses across trials recordings by adaptive kernel estimation (Richmond et al., 1990). After rescaling time with

$$t' = k \int_0^t \lambda_0(u) du$$

in order to obtain a constant rate ($\lambda=1$), the rescaled distribution of inter-spike intervals τ from the experimental data could be fitted by a homogeneous Gamma distribution (Kuffler et al., 1957)

$$p(\tau) = \frac{\lambda^k \tau^{k-1} e^{-\lambda\tau}}{\Gamma(k)}$$

with fixed rate $\lambda=1$, shape parameter k and the gamma function $\Gamma(k)$. The shape parameter was determined from the moments (mean and variance) of the empirical rescaled distribution of the inter-spike intervals (Barlow et al., 1957; Barbieri et al., 2001)

$$k = \bar{\tau}^2 / \sigma_\tau^2.$$

Simulation results

The fitted parameters for the cell encircled in Figs. 8A,B were $k=2$, $\kappa=2.3$, $f=59$ Hz, $\sigma_f=2$ Hz and $\mu=0$. The QPG model reproduced the multi-peaked distribution of inter-spike intervals and the location of the tallest peak (near 17 ms) that were observed empirically, compare Fig. 9B and Fig. 2A.

We then used the QPG model to estimate the rate at which information was transmitted. To reproduce the differences in phases among trials, we randomized the phase offset ϕ_0 for each one. Again, the simulations resembled the empirical results, compare Fig. 10A with Fig. 6 and Fig. 10C with Fig. 6C. Next, to simulate information rates and spectra after de-jittering, we fixed the phase offset ϕ_0 in the model for all trials. Once more, the QPG model reproduced the experimental results. This similarity is seen in the shape of the spectra and in the information rate (compare Fig. 10B with Fig. 6B); the total upper bounds in bit per spike before (0.51, model and 0.44, experiment) and after de-jittering (1.66, model and 1.62, experiment).

Finally, we used the QPG model to generate surrogate datasets that comprised many more trials than could be acquired with whole-cell recording in vivo. We applied the direct method to the simulated datasets to compare information rates before and after de-jittering, Figs. 10C, D. This analysis supported our conclusion that neural oscillations carry information downstream. That is, the information rate was 0.6 bit/spike (linear extrapolation to zero bin, Fig. 10C dashed line) when the phase of the oscillations was random across trials but grew to 1.8 bit/spike, when the phase of the oscillations phase was aligned across trials, Fig. 10D, dotted line.

Acknowledgments

We thank the former members of the Redwood Neuroscience Institute for discussions and are grateful to Matthias Bethge, Tim Blanche, Yang Dan, Bartlett Mel, Bruno Olshausen, Jascha Sohl-Dickstein, and David Warland for comments on previous versions of the manuscript. This work was supported by the National Institutes of Health (JAH, grant NIH EY09593), and the Redwood Neuroscience Institute (FTS). The clustering of intracellular events was performed using the Klustakwik (Harris et al., 2000) program. The receptive field estimation was done with MATLAB (TM) programming language. The remaining analysis was performed using IPython (Pérez and Granger, 2007) and NumPy/SciPy (Oliphant, 2006, 2007), an open-source software environment written in Python. All figures were produced using Matplotlib (Barrett et al., 2005).

Author Contributions

KK conceived the idea for the project and developed as well as conducted the main analyses of the data. XW, YW and VV developed methods to detect events in the intracellular signal and, with JAH, performed the experiments. QW and XW contributed software for stimulus presentation, data collection and analysis. DLR and WMU performed the extracellular experiments. FTS supervised the project at both sites and contributed to both the theoretical analyses and the development of new methods to analyze the data. The manuscript was written by KK, FTS and JAH.

References

- Ahissar, E. and Vaadia, E. (1990). Oscillatory activity of single units in a somatosensory cortex of an awake monkey and their possible role in texture analysis. *Proceedings of the National Academy of Sciences of the United States of America*, 87(22):8935–9.
- Aldworth, Z., Miller, J., Gedeon, T., Cummins, G., and Dimitrov, A. (2005). Dejittered Spike-Conditioned Stimulus Waveforms Yield Improved Estimates of Neuronal Feature Selectivity and Spike-Timing Precision of Sensory Interneurons. *Journal of Neuroscience*, 25(22):5323–32.
- Arai, I., Yamada, Y., Asaka, T., and Tachibana, M. (2004). Light-Evoked Oscillatory Discharges in Retinal Ganglion Cells Are Generated by Rhythmic Synaptic Inputs. *Journal of Neurophysiology*, 92(2):715–25.

- Barbieri, R., Quirk, M., Frank, L., Wilson, M., and Brown, E. (2001). Construction and analysis of non-Poisson stimulus-response models of neural spiking activity. *Journal of Neuroscience Methods*, 105(1):25–37.
- Barlow, H., Fitzhugh, R., and Kuffler, S. (1957). Change of organization in the receptive fields of the cat's retina during dark adaptation. *The Journal of Physiology*, 137(3):338–54.
- Barrett, P., Hunter, J., Miller, J., Hsu, J., and Greenfield, P. (2005). matplotlib—A Portable Python Plotting Package. *Astronomical Data Analysis Software and Systems XIV ASP Conference Series*, 347:91–95.
- Bialek, W., Rieke, F., de Ruyter van Steveninck, R., and Warland, D. (1991). Reading a neural code. *Science*, 252(5014):1854–57.
- Borst, A. and Theunissen, F. (1999). Information theory and neural coding. *Nature Neuroscience*, 2:947–57.
- Brenner, N., Strong, S., Koberle, R., Bialek, W., and Steveninck, R. (2000). Synergy in a Neural Code. *Neural Computation*, 12(7):1531–52.
- Brivanlou, I., Warland, D., and Meister, M. (1998). Mechanisms of concerted firing among retinal ganglion cells. *Neuron*, 20(3):527–39.
- Bruno, R. and Sakmann, B. (2006). Cortex Is Driven by Weak but Synchronously Active Thalamocortical Synapses. *Science*, 312(5780):1622–1627.
- Butts, D., Weng, C., Jin, J., Yeh, C., Lesica, N., Alonso, J., and Stanley, G. (2007). Temporal precision in the neural code and the timescales of natural vision. *Nature*, 449(7158):92–95.
- Castelo-Branco, M., Neuenschwander, S., and Singer, W. (1998). Synchronization of Visual Responses between the Cortex, Lateral Geniculate Nucleus, and Retina in the Anesthetized Cat. *Journal of Neuroscience*, 18(16):6395–410.
- Dan, Y., Atick, J., and Reid, R. (1996). Efficient Coding of Natural Scenes in the Lateral Geniculate Nucleus: Experimental Test of a Computational Theory. *Journal of Neuroscience*, 16(10):3351–62.
- Doty, R., Kimura, D., and Mogenson, G. (1964). Photically and Electrically Elicited Responses in the Central Visual System of the Squirrel Monkey. *Experimental neurology*, 10:19–51.
- Eckhorn, R. and Popel, B. (1975). Rigorous and extended application of information theory to the afferent visual system of the cat. II. Experimental results. *Biol Cybern*, 17(1):71–7.
- Fellous, J., Houweling, A., Modi, R., Rao, R., Tiesinga, P., and Sejnowski, T. (2001). Frequency dependence of spike timing reliability in cortical pyramidal cells and interneurons. *J Neurophysiol*, 85(4):1782–7.
- Friedrich, R., Habermann, C., and Laurent, G. (2004). Multiplexing using synchrony in the zebrafish olfactory bulb. *Nature Neuroscience*, 7(8):862–71.
- Fries, P., Nikolić, D., and Singer, W. (2007). The gamma cycle. *Trends in Neurosciences*, 30(7):309–16.
- Frishman, L. and Levine, M. (1983). Statistics of the maintained discharge of cat retinal ganglion cells. *The Journal of Physiology*, 339(1):475–94.
- Gilbert, C. (1977). Laminar differences in receptive field properties of cells in cat primary visual cortex. *The Journal of Physiology*, 268(2):391–421.
- Gollisch, T. and Meister, M. (2008). Rapid Neural Coding in the Retina with Relative Spike Latencies. *Science*, 319(5866):1108–11.

- Granseth, B. and Lindstrom, S. (2003). Unitary EPSCs of Corticogeniculate Fibers in the Rat Dorsal Lateral Geniculate Nucleus In Vitro. *Journal of Neurophysiology*, 89(6):2952–60.
- Hamos, J., Van Horn, S., Raczkowski, D., Uhrlich, D., and Sherman, S. (1985). Synaptic connectivity of a local circuit neurone in lateral geniculate nucleus of the cat. *Nature*, 317(6038):618–21.
- Harris, K., Henze, D., Csicsvari, J., Hirase, H., and Buzsaki, G. (2000). Accuracy of Tetrode Spike Separation as Determined by Simultaneous Intracellular and Extracellular Measurements. *Journal of Neurophysiology*, 84(1):401–14.
- Heiss, W. and Borsnschein, H. (1965). Distribution of impulse of continuous activity of single optic nerve fibers. Effects of light, ischemia, strychnine and barbiturate. *Pflugers Arch Gesamte Physiol Menschen Tiere*, 286(1):1–18.
- Heiss, W. and Borsnschein, H. (1966). Multimodal interval histograms of the continuous activity of retinal cat neurons. *Kybernetik*, 3(4):187–91.
- Hirsch, J., Alonso, J., Reid, R., and Martinez, L. (1998). Synaptic Integration in Striate Cortical Simple Cells. *Journal of Neuroscience*, 18(22):9517–28.
- Hutcheon, B. and Yarom, Y. (2000). Resonance, oscillation and the intrinsic frequency preferences of neurons. *Trends in Neurosciences*, 23(5):216–222.
- Ishikane, H., Gangi, M., Honda, S., and Tachibana, M. (2005). Synchronized retinal oscillations encode essential information for escape behavior in frogs. *Nat Neurosci*, 8(8):1087–95.
- Jarvis, M. and Mitra, P. (2001). Sampling Properties of the Spectrum and Coherency of Sequences of Action Potentials. *Neural Computation*, 13(4):717–49.
- Kenyon, G., Theiler, J., George, J., Travis, B., and Marshak, D. (2004). Correlated firing improves stimulus discrimination in a retinal model. *Neural Computation*, 16(11):2261–91.
- Klein, S. (1992). *Optimizing the estimation of nonlinear kernels*, pages 109–70. CRC Press, Boca Raton.
- Koepsell, K. and Sommer, F. (2008). Information transmission in oscillatory neural activity. *Biological Cybernetics*, 99:403–416.
- Kuffler, S., Fitzhugh, R., and Barlow, H. (1957). Maintained activity in the cat's retina in light and darkness. *J Gen Physiol*, 40(5):683–702.
- Laufer, M. and Verzeano, M. (1967). Periodic activity in the visual system of the cat. *Vision Res*, 7(3):215–29.
- Liu, R., Tzonev, S., Rebrik, S., and Miller, K. (2001). Variability and Information in a Neural Code of the Cat Lateral Geniculate Nucleus. *Journal of Neurophysiology*, 86(6):2789–806.
- Machens, C., Wehr, M., and Zador, A. (2004). Linearity of Cortical Receptive Fields Measured with Natural Sounds. *Journal of Neuroscience*, 24(5):1089–100.
- McClurkin, J., Gawne, T., Richmond, B., Optican, L., and Robinson, D. (1991). Lateral geniculate neurons in behaving primates. I. Responses to two-dimensional stimuli. *Journal of Neurophysiology*, 66(3):777–793.
- Meister, M., Lagnado, L., and Baylor, D. (1995). Concerted Signaling by Retinal Ganglion Cells. *Science*, 270(5239):1207–10.
- Montemurro, M., Rasch, M., Murayama, Y., Logothetis, N., and Panzeri, S. (2008). Phase-of-Firing Coding of Natural Visual Stimuli in Primary Visual Cortex. *Current Biology*, 8(5):375–80.
- Muresan, R., Jurjut, O., Moca, V., Singer, W., and Nikolic, D. (2008). The Oscillation Score: An Efficient Method for Estimating Oscillation Strength in Neuronal Activity. *Journal of Neurophysiology*, 99(3):1333–53.

- Navon, D. (1977). Forest before trees: The precedence of global features in visual perception. *Cognitive Psychology*, 9(3):353–83.
- Neuenschwander, S. and Singer, W. (1996). Long-range synchronization of oscillatory light responses in the cat retina and lateral geniculate nucleus. *Nature*, 379(6567):728–33.
- Nowak, L., Sanchez-Vives, M., and McCormick, D. (1997). Influence of low and high frequency inputs on spike timing in visual cortical neurons. *Cereb Cortex*, 7(6):487–501.
- Oliphant, T. (2006). *Guide to NumPy*. Trelgol.
- Oliphant, T. (2007). Python for Scientific Computing. *Computing in Science & Engineering*, 9(3):10–20.
- OKeefe, J. and Recce, M. (1993). Phase relationship between hippocampal place units and the EEG theta rhythm. *Hippocampus*, 3(3):317–30.
- Pérez, F. and Granger, B. (2007). IPython: A System for Interactive Scientific Computing. *Computing in Science & Engineering*, 9(3):21–29.
- Reich, D. S., Victor, J. D., Knight, B. W., Ozaki, T., and Kaplan, E. (1997). Response variability and timing precision of neuronal spike trains in vivo. *Journal of neurophysiology*, 77(5):2836–41.
- Reinagel, P. and Reid, R. (2000). Temporal Coding of Visual Information in the Thalamus. *Journal of Neuroscience*, 20(14):5392–400.
- Richmond, B., Optican, L., and Spitzer, H. (1990). Temporal encoding of two-dimensional patterns by single units in primate primary visual cortex. I. Stimulus-response relations. *Journal of Neurophysiology*, 64(2):351–69.
- Rieke, F., Warland, D., van Steveninck, R., and Bialek, W. (1999). *Spikes: exploring the neural code*. MIT Press, Cambridge.
- Ruderman, D. and Bialek, W. (1994). Statistics of natural images: Scaling in the woods. *Physical Review Letters*, 73(6):814–17.
- Sahani, M. and Linden, J. (2003). Evidence Optimization Techniques for Estimating Stimulus-Response Functions. In S. Becker, S. Thrun, K. O., editor, *Advances in Neural Information Processing Systems 15: Proceedings of the 2002 Conference*, pages 109–16. MIT Press.
- Stephens, G., Neuenschwander, S., George, J., Singer, W., and Kenyon, G. (2006). See globally, spike locally: oscillations in a retinal model encode large visual features. *Biological Cybernetics*, 95(4):327–48.
- Szwed, M., Bagdasarian, K., and Ahissar, E. (2003). Encoding of Vibrissal Active Touch. *Neuron*, 40(3):621–630.
- Torralba, A. (2003). Contextual Priming for Object Detection. *International Journal of Computer Vision*, 53(2):169–91.
- Usrey, W., Reppas, J., and Reid, R. (1998). Paired-spike interactions and synaptic efficacy of retinal inputs to the thalamus. *Nature*, 395(6700):384–7.
- Usrey, W., Reppas, J., and Reid, R. (1999). Specificity and Strength of Retinogeniculate Connections. *Journal of Neurophysiology*, 82(6):3527–40.
- Wang, X., Wei, Y., Vaingankar, V., Wang, Q., Koepsell, K., Sommer, F., and Hirsch, J. (2007). Feedforward Excitation and Inhibition Evoke Dual Modes of Firing in the Cat’s Visual Thalamus during Naturalistic Viewing. *Neuron*, 55(3):465–78.
- Williams, P., Mechler, F., Gordon, J., Shapley, R., and Hawken, M. (2004). Entrainment to Video Displays in Primary Visual Cortex of Macaque and Humans. *Journal of Neuroscience*, 24(38):8278–88.

Wollman, D. and Palmer, L. (1995). Phase locking of neuronal responses to the vertical refresh of computer display monitors in cat lateral geniculate nucleus and striate cortex. *Journal of Neuroscience Methods*, 60(1-2):107-13.